Macroscopic entanglement and violation of Bell's inequalities between two spatially separated quantum dots in a planar photonic crystal system

P. Yao and S. Hughes

Department of Physics, Queen's University
Kingston, ON K7L 3N6, Canada
shughes@physics.queensu.ca

Abstract: We present and apply a medium-dependent quantum optics formalism for describing the exciton dynamics of two spatially-separated quantum dots on-chip, in the regime of coupled-cavity quantum electrodynamics. With each dot placed in a spatially-separated cavity and coupled through a periodic waveguide channel, the quantum dot excitons behave as a composite entangled pair, exhibiting pronounced entanglement over distances of 300 μm and more. The computed light spectra above the two cavities show clear signatures of pronounced photon coupling including increased vacuum Rabi splitting and cavity-induced transmission and absorption. The macroscopic entanglement is confirmed by investigating the Bell inequality, which is shown to be violated for hundreds of picoseconds.

OCIS codes: (270.5580) Quantum electrodynamics; (350.4238) Nanophotonics and photonic crystals.

References and links

1. A. K. Ekert, "Quantum cryptography based on Bell's theorem," Phys. Rev. Lett. **67**, 661 (1991).
2. C. H. Bennett, G. Brassard, C. Crépeau, R. Jozsa, A. Peres, and W. K. Wootters, "Teleporting an unknown quantum state via dual classical and Einstein-Podolsky-Rosen channels," Phys. Rev. Lett. **70**, 1895 (1993).
3. C. H. Bennett and S. J. Wiesner, "Communication via one- and two-particle operators on Einstein-Podolsky-Rosen states," Phys. Rev. Lett. **69**, 2881 (1992).
4. J. Vučković and Y. Yamamoto, "Photonic crystal microcavities for cavity quantum electrodynamics with a single quantum dot," Appl. Phys. Lett. **82**, 2374 (2003).
5. W. Chang, W-Y. Chen, H-S. Chang, T-P. Hsieh, J-I. Chyi, and T-M. Hsu, "Efficient single-photon sources based on low-density quantum dots in photonic-crystal nanocavities," Phys. Rev. Lett. **96**, 117401 (2006).
6. K. Hennessy, A. Badolato, M. Winger, D. Gerace, M. Atatüre, S. Gulde, S. Fält, E. L. Hu, and A. Imamoğlu, "Quantum nature of a strongly coupled single quantum dot cavity system," Nature **445,** 896 (2007).
7. D. Englund, D. Fattal, E. Waks, G. Solomon, B. Zhang, T. Nakaoka, Y. Arakawa, Y. Yamamoto, and J. Vučković, "Controlling the spontaneous emission rate of single quantum dots in a two-dimensional photonic crystal," Phys. Rev. Lett. **95**, 013904 (2005).
8. T. Yoshie, A. Scherer, J. Hendrickson, G. Khitrova, H. M. Gibbs, G. Rupper, C. Ell, O. B. Shchekin, and D. G. Deppe, "Vacuum Rabi splitting with a single quantum dot in a photonic crystal nanocavity," Nature **432**, 200 (2004).
9. J. P. Reithmaier, G. Sek, A. Löffler, C. Hofmann, S. Kuhn, S. Reitzenstein, L. V. Keldysh, V. D. Kulakovskii, T. L. Reinecke, and A. Forchel, "Strong coupling in a single quantum dot semiconductor microcavity system," Nature **432**, 197 (2004).
10. E. Peter, P. Senellart, D. Martrou, A. Lemaitre, J. Hours, J. M. Gérard, and J. Bloch, "Exciton-photon strong-coupling regime for a single quantum dot embedded in a microcavity," Phys. Rev. Lett. **95**, 067401 (2005).

#109910 - $15.00 USD Received 9 Apr 2009; revised 12 Jun 2009; accepted 18 Jun 2009; published 24 Jun 2009

11. S. Hughes and H. Kamada, "Single-quantum-dot strong coupling in a semiconductor photonic crystal nanocavity side coupled to a waveguide," Phys. Rev. B **70**, 195313 (2004).
12. D. Englund, A. Faraon, I. Fushman, N. Stoltz, P. Petroff, and J. Vučković, "Controlling cavity reflectivity with a single quantum dot," Nature **450**, 857 (2007).
13. S. Hughes, "Modified spontaneous emission and qubit entanglement from dipole-coupled quantum dots in a photonic crystal nanocavity," Phys. Rev. Lett. **94**, 227402 (2005)
14. M. Bayer, P. Hawrylak, K. Hinzer, S. Fafard, M. Korkusinski, Z. R. Wasilewski, O. Stern, and A. Forchel, "Coupling and entangling of quantum states in quantum dot molecules," Science **291**, 451 (2001).
15. G. Bester, A. Zunger, and J. Shumway "Broken symmetry and quantum entanglement of an exciton in $In_xGa_{1-x}AsGaAs$ quantum dot molecules," Phys. Rev. B **71**, 075325 (2005).
16. Y. Akahane, T. Asano, B. S. Song, and S. Noda, "High-Q photonic nanocavity in a two-dimensional photonic crystal," Nature **425**, 944 (2003).
17. M. Wubs, L. G. Suttorp, and A. Lagendijk, "Multiple-scattering approach to interatomic interactions and superradiance in inhomogeneous dielectrics," Phys. Rev. A **70**, 053823 (2004).
18. S. Hughes, "Coupled-cavity QED using planar photonic crystals," Phys. Rev. Lett. **98**, 083603 (2007).
19. S. Hughes, H. Gotoh, and H. Kamada, "Classical and quantum optical correlation effects between single quantum dots: the role of the hopping photon," Phys. Rev. B **74**, 115334 (2006).
20. A. Cowan and J. F. Young, "Optical bistability involving photonic crystal microcavities and Fano line shapes," Phys. Rev. E **68**, 46606 (2003).
21. W. K. Wootters, "Entanglement of formation of an arbitrary state of two qubits," Phys. Rev. Lett. **80**, 2245 (1998).
22. K. L. Silverman, R. P. Mirin, S. T. Cundiff, A. G. Norman, "Direct measurement of polarization resolved transition dipole moment in InGaAs/GaAs quantum dots," Appl. Phys. Lett. **82**, 4552 (2003).
23. T. H. Stievater, Xiaoqin Li, D. G. Steel, D. Gammon, D. S. Katzer, D. Park, C. Piermarocchi, and L. J. Sham, "Rabi oscillations of excitons in single quantum dots," Phys. Rev. Lett. **87**, 133603 (2001).
24. E. Waks and J. Vučković, "Dipole induced transparency in drop-filter cavity-waveguide systems," Phys. Rev. Lett. **96**, 153601 (2006).
25. B. R. Mollow, "Power spectrum of light scattered by two-level systems," Phys.Rev. **188**, 1969 (1969).
26. W. Langbein, P. Borri, and U. Woggon, V. Stavarache, D. Reuter, and A. D. Wieck, "Radiatively limited dephasing in InAs quantum dots," Phys. Rev. B **70**, 033301 (2004).
27. J. S. Bell, "On the problem of hidden variables in quantum mechanics," Physics **1**, 195 (1964).
28. A. Einstein, B. Podolsky, and N. Rosen, "Can quantum-mechanical description of physical reality be considered complete?," Phys. Rev. **47**, 777 (1935).
29. A. Beige, W. J. Munro, and P. L. Knight, "Bell's inequality test with entangled atoms," Phys. Rev. A **62**, 052102 (2000).
30. S. Hughes, L. Ramunno, J. F. Young, and J. E. Sipe, "Extrinsic optical scattering loss in photonic crystal waveguides: role of fabrication disorder and photon group velocity," Phys. Rev. Lett. **94**, 33903 (2005).

1. Introduction

The formation of entanglement between quantum bits (qubits) can produce entangled states, namely non-factorizable composite wave-functions whose separated parts may be correlated over large distances, resulting in what Einstein termed: "spooky action at a distance." Besides fundamental interest, entangled states may be used to realize quantum information protocols such as the transmission of secret messages via quantum key distribution [1], teleportation of quantum information [2], and dense coding [3]. With regard to solid-state qubits, individual semiconductor quantum dots (QDs) have generated much interest as they behave like "artificial atoms" due to their characteristic discrete energy spectra and long excitonic lifetimes. Quantum dots also have a number of other attractive features for generating entangled states: i) they can be fixed in position (unlike atoms), ii) discrete excitons have large optical dipole moments, iii) exciton frequencies are compatible with telecom components, and iv) QDs can be integrated with *on-chip* cavity structures such as those facilitated by planar photonic crystals (PCs) [4–6] [see Fig. (1)].

Significant progress has been made on nanophotonic systems based on single QD-cavity systems, such as the enhancement and suppression of single photon spontaneous emission [7], strong coupling cavity-QED [6, 8–10], and single exciton control of nanocavity reflectivity [11, 12]. Cavity-QED coupling between two QDs in a single PC cavity [13] has also been shown to lead to sizable entanglements for QDs that are coupled nearby to the same cavity

#109910 - $15.00 USD Received 9 Apr 2009; revised 12 Jun 2009; accepted 18 Jun 2009; published 24 Jun 2009

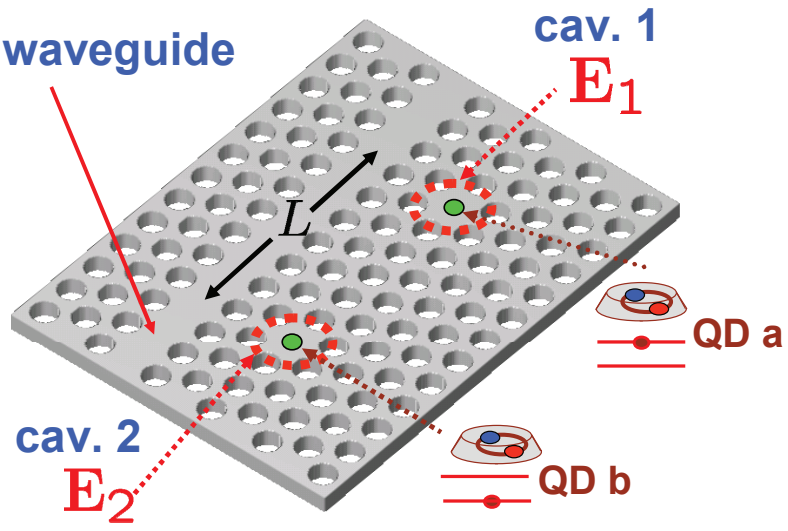

Fig. 1. Schematic diagram of our system, which is composed of two cavities and one waveguide, with one QD in each cavity. The distance between the two cavities is L, and as an example, we show that QD a is initially excited and QD b is in the ground state.

mode; while an interesting scheme, the experimental verification of measuring and using parts of the same composite pair for coupled QDs and proving non-local behavior such as the violation of Bell's inequalities is very difficult. Nevertheless, the proof-of-principle entanglement between spatially separated quantum states in a pair of vertically aligned, self-assembled QDs has been indirectly demonstrated by Bayer *et al.* through investigating the QD emission spectra [14]; the maximum entanglement of the coupled excitons was found to be around 0.8 at an inter-dot separation of only 8.5 nm, which quickly diminishes for larger and smaller inter-dot distances [15]. A major disadvantage of nearby QDs is that it is not possible to individually tune/excite the QD, nor probe the quasi-degenerate excitons separately.

In this work, we propose, and develop the theory for, an integrated solid-state device that enables pronounced entanglement between *macroscopically* separated QDs on-chip. We demonstrate that, with suitably excited QDs in a planar PC medium, long lived entangled states can be maintained, showing the violation of the Bell inequality over hundreds of picoseconds. More fundamentally, this coupled QD system gives rise to rich coupling effects including modified strong coupling regimes of cavity-QED. The structure of interest is depicted above in Fig. 1, which includes two single-mode nanocavities and one coupling waveguide. The nanocavities can be formed by localized defects created within the PC, for example by removing and rearranging two of the air holes [16]. The distance between the two nanocavities is L and no direct coupling is assumed. The PC waveguide and cavity resonances are considered to be deep inside the PC photonic bandgap and the propagating waveguide mode is below the light line (lossless).

2. Theory

To establish a quantitative theory, we closely follow the approach introduced by Wubs *et al.* [17]. Specifically, we adopt a canonical Hamiltonian that quantizes the macroscopic electromagnetic fields, and use the dipole approximation for the QD-medium coupling. We label the two QDs a and b, which are embedded in cavities 1 and 2, respectively. Subsequently, we obtain the multipolar-coupling Hamiltonian:

$$\hat{H} = \sum_{m=a,b} \hbar\Omega_m \hat{\sigma}_m^+ \hat{\sigma}_m^- + \sum_\lambda \hbar\omega_\lambda \hat{a}_\lambda^\dagger \hat{a}_\lambda - i\hbar \sum_{m=a,b;\lambda} (\hat{\sigma}_m^- + \hat{\sigma}_m^+)(g_{m\lambda}\hat{a}_\lambda - g_{m\lambda}^* \hat{a}_\lambda^\dagger), \quad (1)$$

#109910 - $15.00 USD Received 9 Apr 2009; revised 12 Jun 2009; accepted 18 Jun 2009; published 24 Jun 2009

where $\hat{a}_\lambda$ represents the field mode operators and $\hat{\sigma}_m^{+/-}$ are the Pauli operators of the QD excitons; we assume one exciton in the spectral region of interest per QD. In addition, Ω_m is the resonant frequency of each QD, and ω_λ is the eigenfrequency corresponding to the transverse modes of the system ($\mathbf{f}_\lambda(\mathbf{r})$), *excluding* the dots; $g_{m\lambda}$ is the field-dot coupling coefficient, defined through $g_{m\lambda} = \sqrt{\frac{\omega_\lambda}{2\hbar\varepsilon_0}}\boldsymbol{\mu}_m \cdot \mathbf{f}_\lambda(\mathbf{r}_m)$, where $\boldsymbol{\mu}_m = \boldsymbol{n}_m\mu_m$ is the optical dipole moment of the QD electron-hole pair.

The Heisenberg equations of motion for the operators can be derived from $\dot{\hat{O}}_i = -i\hbar^{-1}[\hat{O}_i, \hat{H}]$, yielding dynamical equations for $\hat{a}_\lambda$, $\hat{a}_\lambda^\dagger$, $\hat{\sigma}_m^{+/-}$, and $\hat{\sigma}_{mz} = \hat{\sigma}_m^+\hat{\sigma}_m^- - \hat{\sigma}_m^-\hat{\sigma}_m^+$. In an electron picture, $\hat{\sigma}^+ = \hat{c}_e^\dagger\hat{c}_g$ creates an electron in the excited state (conduction band) and $\hat{\sigma}^- = \hat{c}_e\hat{c}_g^\dagger$ destroys an electron in the excited state [or creates an electron in the ground state (valence band)]; similarly, $\hat{\sigma}^+\hat{\sigma}^- = \hat{c}_e^\dagger\hat{c}_e$, where $\rho_{aa/bb} = \langle\hat{\sigma}_{aa/bb}^+\hat{\sigma}_{aa/bb}^-\rangle$ is the excited state population in each QD. After carrying out the Laplace transform of operators [17], where $\hat{O}_i(\omega) = \int_0^\infty \hat{O}(t)e^{i\omega t}dt$, then

$$\hat{a}_\lambda(\omega) = \frac{i\hat{a}_\lambda(t=0)}{\omega-\omega_\lambda} + \frac{\hbar^{-1}\sum_m g_{m\lambda}^*[\hat{\sigma}_m^-(\omega)+\hat{\sigma}_m^+(\omega)]}{\omega-\omega_\lambda}, \tag{2}$$

$$\hat{a}_\lambda^\dagger(\omega) = \frac{i\hat{a}_\lambda^\dagger(t=0)}{\omega+\omega_\lambda} - \frac{\hbar^{-1}\sum_m g_{m\lambda}[\hat{\sigma}_m^-(\omega)+\hat{\sigma}_m^+(\omega)]}{\omega+\omega_\lambda}, \tag{3}$$

$$\hat{\sigma}_m^-(\omega) = \frac{i\hat{\sigma}_m^-(t=0)}{\omega-\Omega_m} + \frac{\hbar^{-1}\mu_m\hat{E}_\mu(\mathbf{r}_m,\omega)*\hat{\sigma}_{mz}(\omega)}{\omega-\Omega_m}, \tag{4}$$

$$\hat{\sigma}_m^+(\omega) = \frac{i\hat{\sigma}_m^+(t=0)}{\omega+\Omega_m} - \frac{\hbar^{-1}\mu_m\hat{E}_\mu(\mathbf{r}_m,\omega)*\hat{\sigma}_{mz}(\omega)}{\omega+\Omega_m}, \tag{5}$$

$$\hat{\sigma}_{mz}(\omega) = \frac{i\hat{\sigma}_{mz}(t=0)}{\omega} + \frac{2\hbar^{-1}\mu_m\hat{E}_\mu(\mathbf{r}_m)*[\hat{\sigma}_m^-(\omega)-\hat{\sigma}_m^+(\omega)]}{\omega}. \tag{6}$$

Here, $\hat{E}_\mu(\mathbf{r}_m,\omega) = \hat{\mathbf{E}}(\mathbf{r}_m,\omega)\cdot\mathbf{n}_m$, and the symbol '$*$' represents a convolution operator. Using the formal definition of electric-field operator, $\hat{\mathbf{E}}(\mathbf{r},t) = i\sum_\lambda\sqrt{\frac{\hbar\omega_\lambda}{2\varepsilon_0}}\hat{a}_\lambda(t)\mathbf{f}_\lambda(\mathbf{r}) + H.c.$, we obtain the "exact" electric-field operator in frequency space:

$$\begin{aligned}\hat{\mathbf{E}}(\mathbf{r},\omega) &= \hat{\mathbf{E}}_0(\mathbf{r},\omega) + \sum_m \frac{1}{\varepsilon_0}\mathbf{K}(\mathbf{r},\mathbf{r}_m;\omega)\cdot\hat{\mathbf{d}}_m(\omega) \\ &\quad - \sum_m \mathbf{K}(\mathbf{r},\mathbf{r}_m;\omega)\cdot\mathbf{n}_m\alpha_m(\omega)[\hat{E}_\mu(\mathbf{r}_m,\omega)*\hat{\sigma}_{mz}(\omega)],\end{aligned} \tag{7}$$

where $\alpha_m(\omega) = 2\Omega_m\mu_m^2/[\hbar\varepsilon_0(\Omega_m^2-\omega^2)]$ is a *bare* polarizability term, and $\mathbf{K}(\mathbf{r},\mathbf{r}';\omega) = \sum_\lambda \omega_\lambda^2/(\omega_\lambda^2-\omega^2)\mathbf{f}_\lambda(\mathbf{r})[\mathbf{f}_\lambda(\mathbf{r}')]^*$ is a medium Green function [17, 18] in the absence of QDs. To derive the above electric-field operator, we have assumed that the dipole moments are real, and have exploited the fact that, for real ε media, both $\mathbf{f}_\lambda$ and $\mathbf{f}_\lambda^*$ are used per λ in the mode summation. The $\mathbf{K}$ Green function is then obtained only through the transverse modes of the system and is related to the more familiar $\mathbf{G} = \mathbf{G}^{\mathrm{T}} + \mathbf{G}^{\mathrm{L}}$ (including both transverse and longitudinal modes), through [17] $\mathbf{K} = \mathbf{G} + \mathbf{1}\delta(\mathbf{r}-\mathbf{r}')/\varepsilon(\mathbf{r})$, with $\mathbf{1}$ the unit tensor, and $\varepsilon(\mathbf{r})$ is the spatially-dependent dielectric constant. These Green functions are classical and can be defined in the usual way from Maxwell's equations, solved with a polarization dipole. Under the weak excitation approximation, where we consider at most one excitation in the system, and assuming that the ensuing dynamics will be driven by the initially excited QD(s), then the electric-field operator can be expressed explicitly as

$$\hat{\mathbf{E}}(\mathbf{r},\omega) = \sum_{m=a,b}\varepsilon_0^{-1}\mathbf{K}^{(2)}(\mathbf{r},\mathbf{r}_m;\omega)\cdot\hat{\mathbf{d}}_m(\omega), \tag{8}$$

#109910 - $15.00 USD Received 9 Apr 2009; revised 12 Jun 2009; accepted 18 Jun 2009; published 24 Jun 2009

where QD a/b is located at $\mathbf{r}_{a/b}$, and we have introduced the quantum dipole source $\hat{\mathbf{d}}_m(\omega) = i\boldsymbol{\mu}_m\left[\frac{\hat{\sigma}_m^-(t=0)}{\omega-\Omega_m}+\frac{\hat{\sigma}_m^+(t=0)}{\omega+\Omega_m}\right]$, and a *QD-modified* Green function for the medium:

$$\mathbf{K}^{(2)}(\mathbf{r},\mathbf{r}_a;\omega)=\frac{\tilde{\mathbf{K}}(\mathbf{r},\mathbf{r}_a;\omega)+\tilde{\mathbf{K}}(\mathbf{r},\mathbf{r}_b;\omega)\cdot\mathbf{n}_b\,\alpha_b(\omega)\,\mathbf{n}_b\cdot\tilde{\mathbf{K}}(\mathbf{r}_b,\mathbf{r}_a;\omega)}{1-\mathbf{n}_b\cdot\tilde{\mathbf{K}}(\mathbf{r}_a,\mathbf{r}_b;\omega)\cdot\mathbf{n}_b\,\alpha_b(\omega)\,\mathbf{n}_a\cdot\tilde{\mathbf{K}}(\mathbf{r}_b,\mathbf{r}_a;\omega)\cdot\mathbf{n}_a\alpha_a(\omega)}, \tag{9}$$

where $\tilde{\mathbf{K}}(\mathbf{r},\mathbf{r}_m;\omega)=\mathbf{K}(\mathbf{r},\mathbf{r}_m;\omega)/[1-\mathbf{n}_m\cdot\mathbf{K}(\mathbf{r}_m,\mathbf{r}_m;\omega)\cdot\mathbf{n}_m\alpha_m(\omega)]$. We stress that $\mathbf{K}^{(2)}$ *exactly* includes the full dynamical coupling effects between the two QDs, and fully covers both weak and strong coupling regimes in a self-consistent way. Similar expressions have been derived classically for the medium-dependent QD polarizabilities [19], and quantum mechanically for coupled atoms (using a harmonic oscillator model) [17].

Next, we require the classical Green functions for the coupled-cavity planar PC medium. These have been derived before [18], so here we just introduce the main points, and extend the theory for the problem at hand. The analytic Green function for the waveguide-plus-two-cavity medium ($\mathbf{K}_{wcc}$) can be derived by assuming *weakly coupled* cavity-to-waveguide channels and employing a matrix inversion technique [11, 18, 20]. We can conveniently choose different modal components through $\mathbf{K}(\mathbf{r},\mathbf{r}';\omega)=\sum_{\alpha\beta}\langle\mathbf{r}|\mathbf{K}^{\alpha\beta}|\mathbf{r}'\rangle$, where $\mathbf{K}^{\alpha\beta}$ is the projection of $\mathbf{K}$ on $|\mathbf{E}_\alpha\rangle$ from the left and $\langle\mathbf{E}_\beta|$ from the right, and we use the notation $\mathbf{f}_\alpha(\mathbf{r})=\langle\mathbf{r}|\mathbf{E}_\alpha\rangle$ and $\mathbf{f}_\alpha^*(\mathbf{r})=\langle\mathbf{E}_\alpha|\mathbf{r}\rangle$. Assuming a positive group velocity for the waveguide mode ($v_g>0$), example projections include [18]

$$\mathbf{K}_{wcc}^{11}=\frac{\omega^2\,|\mathbf{E}_1\rangle\langle\mathbf{E}_1|}{\omega_1^2-\omega^2-i\omega\Gamma_1^0-i\omega\Gamma_1^w[1+e^{i2k_wL}r_2(\omega)]}, \tag{10}$$

$$\mathbf{K}_{wcc}^{12}=\frac{\omega^2 r_1(\omega)e^{ik_wL}\,|\mathbf{E}_1\rangle\langle\mathbf{E}_2|}{\omega_2^2-\omega^2-i\omega\Gamma_2^0-i\omega\Gamma_2^w[1+e^{i2k_wL}r_1(\omega)]}, \tag{11}$$

where $r_1(\omega)=i\omega\Gamma_1^w/[\omega_1^2-\omega^2-i\omega(\Gamma_1^0+\Gamma_1^w)]$ is the waveguide mode reflection coefficient from cavity 1, Γ_c^w is the cavity-to-waveguide coupling rate whose explicit form depends on the overlap between the cavity mode and the waveguide mode [11], and $\Gamma^0\ll\Gamma_c^w$ is the bare cavity coupling rate caused by coupling to radiation modes above the light line. We note that these functions are not simple Lorenzian lineshapes, and the cavity decay process is a complicated function of frequency and waveguide length L.

The quantum dynamics of the spatially separated qubits can be obtained from the inverse Laplace transform of the QD operators, which in the weak excitation regime has the form

$$\hat{\sigma}_{a/b}^-(\omega) \quad = \quad \frac{i\hat{\sigma}_{a/b}^-(t=0)}{\omega-\omega_{a/b}}+\frac{\hbar^{-1}\boldsymbol{\mu}_{a/b}\cdot\hat{\mathbf{E}}(\mathbf{r}_{a/b},\omega)}{\omega-\omega_{a/b}}. \tag{12}$$

Exploiting the definition of the time-dependent wave function, $|\psi(t)\rangle=\sum_{m=a,b}C_m^u(t)\,|a_m^e,0\rangle+\sum_{m=a,b}C_{m,\lambda}^g(t)\,|a_m^g,\lambda\rangle$, we define the amplitude coefficient of the QD upper excited state as $C_{a/b}^u(t)=\int_{-\infty}^{\infty}\langle 0|\hat{\sigma}_{a/b}^-(\omega)|\psi(t=0)\rangle e^{-i\omega t}d\omega$, with $|0\rangle$ the lower level eigenstate of the QDs. The upper state population of each QD is then obtained from $\rho_{mm}=|C_m^u|^2$.

Finally, we also derive *exact analytical expressions for the light spectrum and the entanglement of formation* [21]. From the first-order quantum correlation function, the spectrum is defined as $S(\mathbf{r},\omega)=\langle(\hat{\mathbf{E}}(\omega))^\dagger\hat{\mathbf{E}}(\omega)\rangle$, yielding

$$S(\mathbf{r},\omega)=\sum_{m=a,b}\frac{|\mathbf{K}^{(2)}(\mathbf{r},\mathbf{r}_m;\omega)\cdot\boldsymbol{\mu}_m|^2}{\varepsilon_0^2}\,\frac{\langle\hat{\sigma}_m^+(t=0)\hat{\sigma}_m^-(t=0)\rangle}{(\omega-\Omega_m)^2}, \tag{13}$$

#109910 - $15.00 USD Received 9 Apr 2009; revised 12 Jun 2009; accepted 18 Jun 2009; published 24 Jun 2009

which can be spatially projected to separately obtain the emitted spectrum detected above cavity 1 and (or) cavity 2. To compute the quantum correlations between the coupled QD qubits, the entanglement of formation is obtained from the concurrence [21], $Con(t)$, through $E(t) = -x\log_2(x) - (1-x)\log_2(1-x)[x = (1+\sqrt{1-Con^2(t)})/2]$, where $Con = |\langle\psi|\tilde{\psi}\rangle|$ (tilde represents a spin flip) [21]. For this we need the reduced density matrix of our two-qubit system ρ, which is obtained by tracing out the electric field modes, where the elements of the wave function $|\psi\rangle$ are obtained from the QD operators, i.e., Eqs. (12) and (8). For our system of interest, where the initial excitation resides in the QDs, the concurrence becomes simply $Con = 2|C_a^u||C_b^u|$.

3. Quantum dynamics, entanglement of formation, and cavity-emitted spectra

For calculations, we use bare quality factors of cavity $Q^0_{1/2}(=\omega_{1/2}/\Gamma^0_{1/2}) = 20\,000$, and a cavity-waveguide quality factor of $Q^w_{1/2}(=\omega_{1/2}/\Gamma^w_{1/2}) = 500$ for both cavities. Increasing $Q^0_{1/2}$ actually has little influence on our results because the decay of PC system is dominated by the coupling between the cavities and the waveguide; and for the regime of coupled-cavity QED [18], the most important parameter is the ratio Γ^w/Γ^0 or Q^0/Q^w. In addition, we choose $\omega_{1/2} = \Omega_{a/b}$, $\hbar\omega_1 = \hbar\Omega_a = 0.95\,\text{eV}$, effective cavity mode volume $V_{c1/c2} = 0.07\,\mu\text{m}^3$, and a background dielectric constant of the PC slab, $\varepsilon_b = 12$; for the QD dipole moments we use parameters similar to those in experiments [22, 23], and first use an *effective* dipole moment $\mu_a = 30\,\text{D}$ (Debye) and $\mu_b = 60\,\text{D}$ (this asymmetry helps to ensure maximum entanglement for QD a initially excited). In practise, the effective dipole moments can be achieved from different orientations, or, equivalently, by different spatial positioning with respect to the cavity field antinode positions; though we could also easily change other parameters within the formalism. We note that, according to the recent fabrication improvements [6], the error of precise spatial positioning of the QD to a cavity field antinode can be less than 10% (so $g_c^{\text{exp}} > 0.9 g_c^{\text{max}}$), and to within this accuracy, we have tested that our proposed scheme is robust. Necessarily taking causality into consideration, the chromatic dispersion of the waveguide is introduced linearly and the group velocity $v_g = d\omega/dk = c/10$; also, unless stated otherwise, the cavity-cavity separation $L = 3 - 300\,\mu\text{m}$, which yield waveguide retardation times of 0.1 ps to 10 ps.

Experimentally, the QDs are usually optically excited far off resonance, and the initial excitons are created *incoherently*. Thus, a suitable initial condition for the two QD system is $|\psi(t=0)\rangle_{QD} = \cos(\theta)|10\rangle + e^{i\phi}\sin(\theta)|01\rangle$, corresponding to an exciton shared between the two dots with the field in vacuum. With only one QD in the system, we assume $|\psi(t=0)\rangle_{QD} = |1\rangle$.

For a reference calculation, we first perform simulations with only 1 QD in the system, with QD b removed, and set $\omega_1 = \omega_2 = \Omega_a$. In Figs. 2(a,c,e), we show the excited QD dynamics for various cavity separation distances of $L = 3, 30,$ and $300\,\mu\text{m}$, respectively. In Fig. 2(a), we clearly see strong coupling phenomena and vacuum Rabi oscillations, which is enhanced over the one cavity result because cavity 2 acts to increase the local density of photon states at the position of QD a (in cavity 1) [18]. Interestingly, for increasing L, the Rabi oscillation period increases (smaller effective cavity coupling), and we eventually recognize weak retardation oscillations in the excited state population dynamics; these oscillations are caused by the single photon being recycled between the two cavities with a period that corresponds to the round trip time of the coupled cavity system. The corresponding emitted spectra from cavity 1 and cavity 2 are shown in Figs. 2(b,d,f), which show that the vacuum Rabi doublet decreases in width as a function of waveguide length L. In this latter case, we highlight that the length $L = 300\,\mu\text{m}$ would correspond to around 700-800 PC unit cells. A clear advantage of our formalism is the ease with which we can study various structural parameters such as waveguide length, where direct numerical approaches would be impractical and cumbersome.

#109910 - $15.00 USD Received 9 Apr 2009; revised 12 Jun 2009; accepted 18 Jun 2009; published 24 Jun 2009

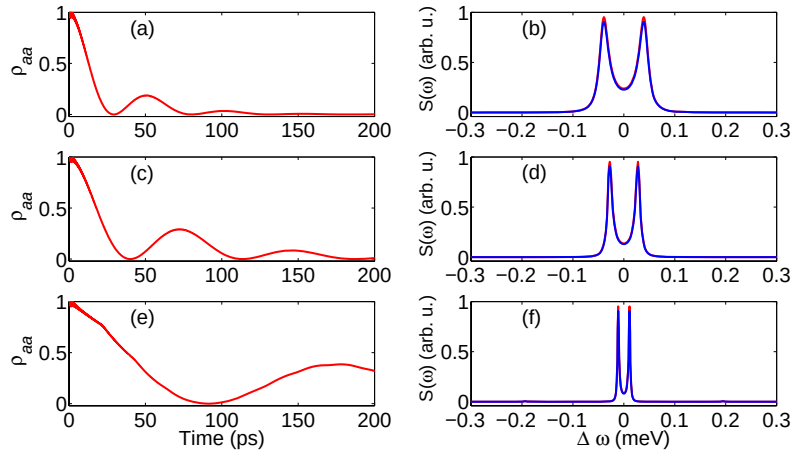

Fig. 2. One QD dynamics and emitted spectra. (a,c,e) Population decay of only one QD (QD b is a removed, and $\mu_a = 30\,\mathrm{D}$), when the cavities are separated by $L = 3$, 30, and 300 μm, respectively; the dot and cavity resonance frequencies are $\omega_{1/2} = \Omega_a$. (b,d,e) Corresponding emitted spectra above cavity 1 and cavity 2, shown by the red and blue curves, respectively; all spectra are normalized to the peak emitted spectrum from cavity 1. Note that the small oscillations slightly visible on the early time dynamics of QD a (first few ps) is a numerical artifact caused by the finite frequency bandwidth used to compute the inverse Laplace transform; it has no effect on the later dynamics or the spectrum.

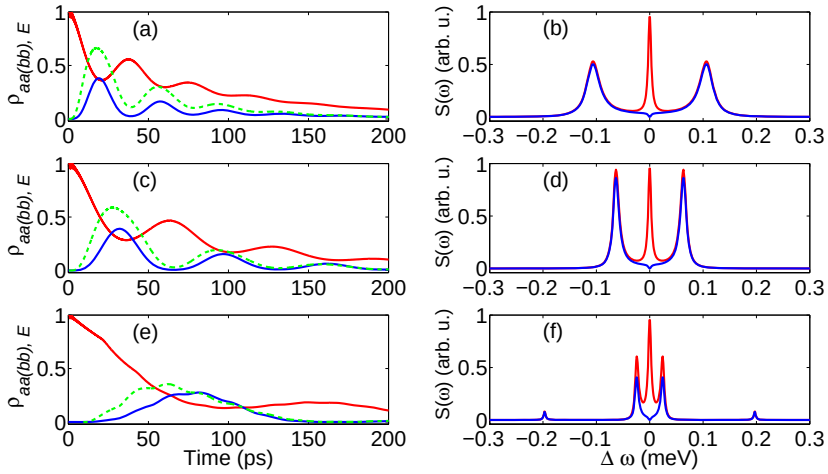

Fig. 3. Two QD dynamics, entanglement of formation, and emitted spectra. (a) Population decay and entanglement when QD a ($\mu_a = 30\,\mathrm{D}$) and QD b ($\mu_b = 60\,\mathrm{D}$) are separated by L=3 μm, with $\omega_{1/2} = \Omega_{a/b}$. The red solid curve (blue solid curve) represents the exciton decay of QD a(b), while the green dashed curve corresponds to the entanglement of formation. (b) Corresponding vertically-emitted spectra, where the solid red curve (solid blue curve) represents the emission spectrum of cavity 1(2). (c-d) as in (a-b) but with $L = 30\,\mu$m. (e-f) As in (a-b) but with $L = 300\,\mu$m.

Next, we explore the two QD dynamics by adding in the second dot b. We study the resonant condition of $\omega_1(=\Omega_a) = \omega_2(=\Omega_b)$, and also the case with detuning, $\omega_1(=\Omega_1) \neq \omega_2(=\Omega_b)$. For both cases, only QD a is initially excited ($C_a^u(0) = 1$, $C_b^u(0) = 0$). The resonant case is shown in Fig. 3, which demonstrates that pronounced entanglement values can be realized (see

#109910 - $15.00 USD Received 9 Apr 2009; revised 12 Jun 2009; accepted 18 Jun 2009; published 24 Jun 2009

Fig. 3(a), green dashed curve), reaching a maximum value of around 0.67 ebits for $L = 3\mu$m. The oscillations in the QD dynamics are caused by both the dot-dot photon exchange interactions and the cavity-dot interactions, and we find that the vacuum Rabi oscillations are much faster than the one QD scenario (cf. red curves in 2(a,c) and 3(a,c)). For the emitted spectra, in addition to the expected vacuum Rabi doublet (now with a significantly larger splitting than before), we also obtain a pronounced constructive or destructive center peak that originates from the photon emission from the excited dot in the *opposite* cavity propagating back and resonantly scattering from the cavity (e.g., the dot in cavity 2 can act as a source for pumping the dot in cavity 1); this is analogous to dipole-induced transparency or dipole-induced absorption [11, 24], where one obtains interference between the excitation field and the field emitted from the excited QD. The lineshape from cavity 1 is also similar to the well-known Mollow triplet [25]. More interestingly, in the context of coupled QDs, we also see an additional doublet (larger splitting of around 0.4 meV for $L = 300\,\mu$m) which is caused by the dynamic photon coupling that takes place from cavity to cavity, as discussed above.The latter spectral doublet give clear evidence to the formation of a macroscopic molecule. Again for the longer cavity separations, the vacuum Rabi oscillations (coherent oscillations) are suppressed, and for $L = 300\,\mu$m, a clear retardation feature of around 10 ps is observed. When L is increased to a larger value of $300\,\mu$m, the entanglement peak is still reasonable (~ 0.3). While the usual coupled-QD entanglement distance between excitons is only about 10 nm, here we obtain a *macroscopic* entanglement by *indirect* cavity-cavity coupling, via the integrated waveguide. Furthermore, this macroscopic entanglement has the added advantage that the coupling phenomena can be probed by measuring the individual cavity-emitted light spectra.

These coherent coupling phenomena naturally become less pronounced in the presence of non-radiative exciton decay and spectral detuning between the cavities and QDs, though significant qubit coupling is still be apparent for a wide range of parameters. For single QDs, at low temperatures of $T = 4$K, even for regular (non-cavity) structures, the exciton relaxation is typically dominated by radiative decay, and the non-radiative decay times (rates) are around 2 ns ($\sim 2\,\mu$eV) [26]; thus, for studying the early time dynamics of the first 500 ps or so, their influence can be approximately neglected. A more significant effect on the QD photon transfer mechanisms would result from detuning between the two QD-cavity sections, though these could be individually tuned to ensure resonance with each QD-cavity pair. As an example, in

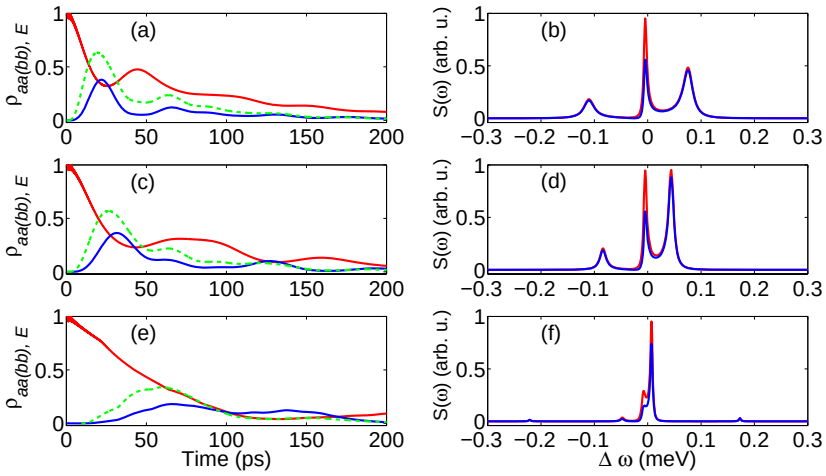

Fig. 4. As in Fig. 3, but with a detuning of $\omega_1(=\Omega_a) - \omega_2(=\Omega_b) = 25\,\mu$eV.

#109910 - $15.00 USD Received 9 Apr 2009; revised 12 Jun 2009; accepted 18 Jun 2009; published 24 Jun 2009

Fig. 4 we add a detuning of $\Omega_a - \Omega_b = 25\,\mu$eV and repeat the same investigation as shown in Fig. 3. While the entanglement and photon coupling effects are reduced, we still obtain significant coupling between the QDs via the coupling waveguide.

4. Bell inequalities

Finally, we address the non-local coupling of our proposed PC system by analyzing the Bell inequality. The Bell inequality [27], if violated, is a proven way to test the EPR paradox [28] and the non-local realism of a coupled quantum state. For quantum spin systems, which mathematically map on to our two-coupled QD excitons, the Bell inequality of interest [29]: $B_s = |E(\theta_a,\theta_b) - E(\theta_a,\theta'_b) + E(\theta'_a,\theta_b) - E(\theta'_a,\theta'_b)| \leq 2$, where the correlation function $E(\theta_a,\theta_b) = \langle \hat{\sigma}_a^{\theta_a} \hat{\sigma}_b^{\theta_b} \rangle$, $\hat{\sigma}_m^{\theta_m} = \cos(\theta_m)\hat{\sigma}_{mx} + \sin(\theta_m)\hat{\sigma}_{my}$, $\hat{\sigma}_{mx} = \hat{\sigma}_m^+ + \hat{\sigma}_m^-$, $\hat{\sigma}_{my} = -i\hat{\sigma}_m^+ + i\hat{\sigma}_m^-$ and $\theta_m(\theta'_m)$ is a real-angle parameter. Thus, if one chooses $\theta = \theta_a - \theta_b = \theta_b - \theta'_a = \theta'_a - \theta'_b$, then above inequality will be simplified to $B_s = |3E(\theta,0) - E(3\theta,0)| \leq 2$, where $E(\theta,0) = e^{i\theta}\langle \hat{\sigma}_a^+ \hat{\sigma}_b^- \rangle + c.c. = C_a^*(t)C_b(t)e^{i[(\Omega_a - \Omega_b)t + \theta]} + c.c.$ The Bell inequality is therefore violated if $B_s > 2$.

One can consider the evolution of an initial maximally-entangled two-qubit state $|\psi\rangle_{QD}^{\pm} = \frac{1}{\sqrt{2}}(|01\rangle \pm |10\rangle)$. The Bell states can in principle be generated by a single photon source, where the single photons are first split by a $50\% - 50\%$ beam splitter, and then undergo a different phase delay (0 or π), which then excite the pair of QDs. More elaborate schemes could, in principle, send in an incident field through a leaky waveguide mode, that could prepare the QDs pair in the correct superposition state. Inspecting the symmetry properties of Eq. (12), is can be recognized that $C_a^u(t) = \pm C_b^u(t)$ if cavity 1 is symmetric with cavity 2 and QD a is resonant with QD b, and their evolution will be governed by the term $\mathbf{K}(\mathbf{r}_{a/b},\mathbf{r}_{a/b};\omega) \pm \mathbf{K}(\mathbf{r}_{b/a},\mathbf{r}_{a/b};\omega)$. The decay of the state $\frac{1}{\sqrt{2}}(|01\rangle + |10\rangle)$ will be faster than $\frac{1}{\sqrt{2}}(|01\rangle - |10\rangle)$ if $\mathbf{K}(\mathbf{r}_a,\mathbf{r}_a;\omega)$ is in phase (interferences constructively) with $\mathbf{K}(\mathbf{r}_a,\mathbf{r}_b;\omega)$. On the contrary, if $\mathbf{K}(\mathbf{r}_a,\mathbf{r}_a;\omega)$ is out of phase (interferences destructively) with $\mathbf{K}(\mathbf{r}_a,\mathbf{r}_b;\omega)$, then the decay of the state $\frac{1}{\sqrt{2}}(|01\rangle - |10\rangle)$ will be faster than $\frac{1}{\sqrt{2}}(|01\rangle + |10\rangle)$. For our waveguide example, the violation time of the Bell inequality for the initial condition $|\psi\rangle_{QD}^-$ is shorter than that of the initial condition $|\psi\rangle_{QD}^+$, which is caused by the *destructive* interference between $\mathbf{K}(\mathbf{r}_a,\mathbf{r}_a;\omega)$ and $\mathbf{K}(\mathbf{r}_a,\mathbf{r}_b;\omega)$. Thus, we will only show the initial condition of $|\psi\rangle_{QD}^+$.

The Bell inequality simulations are summarized in Fig. 5, which display a selection of population and Bell parameter dynamics, for various L and QD dipole moments. To better understand these results, we note that the violation of the Bell inequality for the initial condition $|\psi\rangle_{QD}^+$ is largely insensitive to the distance L, but more sensitive to the dipole moments (or effective dipole moments, as ultimately the coupling is controlled through g_λ). In Fig 5(a-b), we show the QD population dynamics and B_s for a QD dipole of $d_{a/b} = 30\,$D, with $L = 3\,\mu$m (red curve) and $L = 300\,\mu$m (blue curve); the Bell inequality is found to be violated for both waveguide lengths for a timescale of up to 50 ps, with the longer system simply exhibiting more pronounced retardation dynamics (oscillations). When the effective dipole moment reduces from 30 D to 8 D, the violation time increases from around 50 ps to more than 800 ps (see Fig. 5(d)).

For a detuning of $25\,\mu$eV, then this violation is reduced to around 200-300 ps (see Fig.5(f)), though can be increased by having a larger L. There is also an interesting entanglement revival for the longer waveguide, where the B_s increases about 400 ps. Note that for sufficiently large L, one must be careful of disorder-induced losses in the PC waveguide [30], though an increased entanglement duration can also be achieved by using smaller dipole moments or dots that are not maximally positioned on the cavity antinode, since this reduces the radiative decay; in this case, the ultimate limit will likely come from the non-radiative decay processes such as electron-phonon scattering, which we have neglected in this study. With the appropriate PC

#109910 - $15.00 USD Received 9 Apr 2009; revised 12 Jun 2009; accepted 18 Jun 2009; published 24 Jun 2009

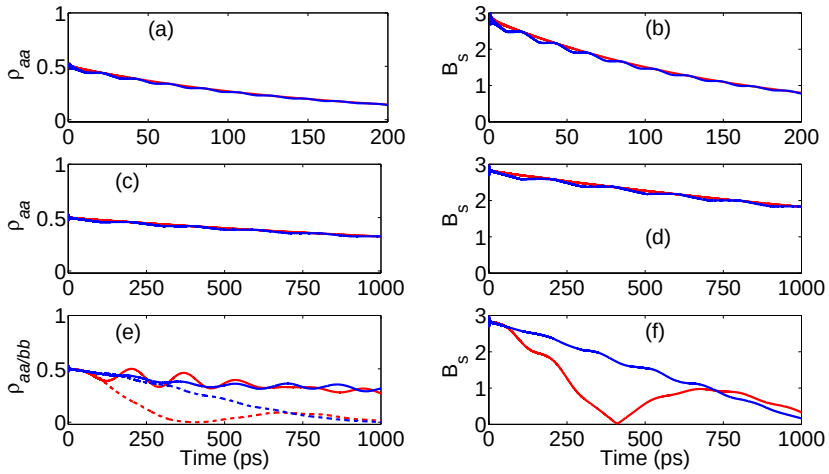

Fig. 5. Decay of a maximally entangled state and the violation of the Bell inequality ($B_s > 2$). Temporal decay of ρ_{aa} (a,c,e) and B_s (b,d,f), with the initial condition of $|\psi_{QD}(t=0)\rangle = |\psi^+_{QD}\rangle$ (see text); note that in (e), ρ_{aa} is shown by the solid curve and ρ_{bb} is shown by the dashed curve, but in (a) and (c), $\rho_{bb} = \rho_{aa}$, so we only show one curve for both. (a-b) $\mu_a = \mu_b = 30\,\mathrm{D}$ and $L = 3\,\mu\mathrm{m}$ (red curves) and $L = 300\,\mu\mathrm{m}$ (blue curves). (c-d) $\mu_a = \mu_b = 8\,\mathrm{D}$ and $L = 300\,\mu\mathrm{m}$ (red curves) and $L = 3000\,\mu\mathrm{m}$ (3 mm) (blue curves). (e-f) As in (c-d) but with a detuning of $\omega_1(=\Omega_a) - \omega_2(=\Omega_b) = 25\,\mu\mathrm{eV}$.

medium coupling, we expect that the entanglement dynamics will be robust for up to several hundred picoseconds using experimentally accessible parameters.

5. Conclusions

We have introduced a novel coupled-cavity QED scheme that can entangle two spatially separated QDs over macroscopic distances. By first developing an essentially exact photon Green-function technique, we have presented analytical formulas for the important system operators and experimental observables, allowing one to investigate a wide range of QD coupling scenarios in a remarkably simplistic and intuitive way – including the full non-Markovian dynamics. We find that effective "QD molecules" can be formed over several hundred microns and more, and that rich dot-cavity and dot-dot coupling dynamics occurs that can be observed indirectly by looking at the emitted light spectrum above each dot-cavity pair. The coupled-cavity QED technique also facilitates a way to test the violation of the Bell inequality using planar PC chips and two QDs that can be fixed in position, locally tuned, and separately probed experimentally.

Acknowledgements

This work was supported by the National Sciences and Engineering Research Council of Canada and the Canadian Foundation for Innovation. We thank Martijn Wubs and Jeff Young for useful discussions.

#109910 - $15.00 USD Received 9 Apr 2009; revised 12 Jun 2009; accepted 18 Jun 2009; published 24 Jun 2009